

# 1 Amphiphilic Nanohybrid Catalysts for Reactions at the Water/Oil Interface in Subsurface Reservoirs

3 Santiago Drexler, Jimmy Faria, M. Pilar Ruiz, Jeffrey H. Harwell, and Daniel E. Resasco\*

4 School of Chemical, Biological, and Materials Engineering, University of Oklahoma, Norman, Oklahoma 73019, United States

5 **ABSTRACT:** A novel technique is proposed for potential use in oil reservoirs. The technique consists in incorporating  
6 amphiphilic nanoparticles into the water injection. These hybrid nanoparticles can simultaneously act as emulsion stabilizers as  
7 well as carriers for catalytic species, e.g., metals. They can be active for in situ reactions, such as partial oxidation and  
8 hydrogenation, which may result in changes in rheological and interfacial properties of the oil, as well as modifying the wettability  
9 of the walls. These changes might be efficiently used to improve the oil recovery process. Specifically, partial oxidation of organic  
10 compounds lowers the water–oil interfacial tension and consequently increases the capillary number ( $N_c$ ) of the system.  
11 Alternatively, partial hydrogenation of polynuclear aromatics can enhance the viscosity of the oil phase in the emulsion, thus  
12 improving the mobility ratio (MR). In addition, partial hydrogenation can be an effective pretreatment of the oil to favor the  
13 subsequent partial oxidation.

## 1. INTRODUCTION

14 Production from large oil fields is stopped many times when  
15 extraction becomes uneconomic, even though a significant  
16 fraction of the original oil in place (OOIP) has not yet been  
17 recovered.<sup>1</sup> Development of alternative techniques to recover  
18 greater amounts of oil economically is an important challenge  
19 for engineers and researchers working in the oil industry. The  
20 incorporation of chemicals into the oil well as part of Enhanced  
21 Oil Recovery (EOR) strategies has been investigated for several  
22 decades.<sup>2</sup>

23 Recently, researchers have started to evaluate the potential  
24 impact of nanotechnology in subsurface reservoir character-  
25 ization and oil recovery.<sup>3–5</sup> In addition to the traditional  
26 phenomena, involving capillary, viscous, and gravitational  
27 forces, researchers are investigating the role of nanoscale  
28 interactions (electro-steric effects) in reservoir operations. It is  
29 believed that nanotechnology has the potential to transform the  
30 modeling and application of chemical EOR. As an example of  
31 these activities, researchers have proposed the use of nano-  
32 particles to modify the wettability of porous media, which  
33 would alter the interaction between the rock and the fluids,  
34 increasing oil recovery (e.g., by increasing the relative  
35 permeability of the oil).<sup>6</sup> In addition, the use of nanoparticles  
36 to reduce the oil–water interfacial tension (IFT) and enhance  
37 the recovery of oil has been experimentally tested.<sup>7</sup> It has been  
38 claimed that, by using a combination of nanoparticles and an  
39 anionic surfactant, a decrease in IFT is obtained, which is ~70%  
40 greater than that reached using the surfactant alone. Moreover,  
41 when the same combination of particles and surfactant was  
42 used in packed columns, a 10% increase in oil recovery was  
43 obtained, compared to that obtained without particles. Other  
44 authors are investigating nanoparticles as contrast agents for the  
45 detection of the water/oil interface in the reservoir and  
46 visualization of residual oil.<sup>3</sup>

47 Two major variables that may have a direct impact in the  
48 EOR process and can be modified by the addition of different  
49 chemicals and particles are the capillary number ( $N_c$ ) and the

mobility ratio (MR).<sup>8</sup> The capillary number is defined as  $N_c =$  50  
 $v\mu/\sigma$ , where  $v$  is the Darcy velocity (fluid flux per unit of area),  $\mu$  51  
the viscosity of the mobilizing fluid (water), and  $\sigma$  the interfacial 52  
tension (IFT) between the oil and the water. Typical  $N_c$  values 53  
are  $\sim 10^{-7}$  after water flooding.<sup>1</sup> The injection of surfactants to 54  
reduce the oil–water IFT has been practiced for more than 55  
35 years.<sup>2,9</sup> Surfactant formulations based on alcohols dissolved 56  
in polyglycoside are generally very effective for enhancing oil 57  
recovery. In addition to decreasing the oil–water IFT, emulsifiers 58  
act as stabilizers of the interface, leading to a greater interfacial 59  
area and a decrease in the capillary forces that act on the oil 60  
inside the pores.<sup>10</sup> Both wettability and entry pressure 61  
requirements affect the displacement of oil by water. When the 62  
rock is water-wet, spontaneous imbibition of the rock displaces 63  
oil from the pores. In addition, if during drainage the pressure 64  
gradient exceeds the required entry pressure (proportional to 65  
oil–water IFT) for the water, the displacement of oil from larger 66  
pores can be achieved at lower pressure gradients by decreasing 67  
the IFT.<sup>11</sup> 68

The mobility ratio (MR) is a function of the relative 69  
permeability ( $k_i$ ) of the porous media toward oil and water, 70  
respectively, and the viscosity ( $\mu_i$ ) of the oil and the mobilizing 71  
fluid (water), respectively: 72

$$\text{MR} = \frac{(k_w/k_o)}{(\mu_w/\mu_o)}$$

To achieve displacement of the oil by the water, MR must be 73  
lower than unity.<sup>12</sup> This condition can be obtained by increas- 74  
ing the viscosity of the sweeping fluid, relative to that of the 75  
oil, since a high  $\mu_w/\mu_o$  value is favorable for oil displacement.<sup>13</sup> 76  
The effectiveness of the different polymers employed is 77  
dependent on their chemical structure and their interaction 78  
with the surfactants and alkalis used for IFT reduction, as 79

Received: January 19, 2012

Revised: March 7, 2012

80 well as their impact on apparent viscosity. For example,  
81 hydrolyzed polyacrylamide and Xanthan gum are examples  
82 of polymers that have been widely studied for EOR appli-  
83 cations. In these studies, the rheology of the aqueous solu-  
84 tions of these polymers combined with anionic surfactants and  
85 alkali has been investigated. It was found that, by using  
86 adequate concentrations, viscosities as high as 210 cP could be  
87 reached.<sup>14</sup>

88 Oil-in-water (O-in-W) emulsions can be produced by  
89 addition of surfactants, which can improve the mobility of the  
90 oil by increasing the sweep efficiency. By changing the oil/water  
91 ratio and the salinity of the water, different emulsion types  
92 (either O-in-W or W-in-O) can be obtained. The rheological  
93 and interfacial properties are affected by these changes, which  
94 may result in enhanced oil recovery and variations in pressure  
95 drop, as measured in sand pack flood studies.<sup>15</sup> Effect of pore  
96 blocking and diversion of injection fluids caused by addition of  
97 silica nanoparticles have been investigated in multiphase flow  
98 experiments in core floods. It has been observed that even  
99 though particles may propagate through sandstone cores, an  
100 addition of polymers usually is required to mobilize residual  
101 oil effectively.<sup>16</sup>

102 Silica nanoparticles have been widely studied as stabilizers of  
103 Pickering emulsions for different applications. In a series of  
104 articles, Binks et al.<sup>17–25</sup> have described systematic studies of  
105 the formation, stability, and structure of this type of emulsion.  
106 They represent a novel alternative to conventional emulsions  
107 and may prove to be advantageous in subsurface oil reservoir  
108 applications, because of their higher thermal and mechanical  
109 stability. By functionalizing the surface of the silica particles  
110 with silanol groups, the hydrophilic–lipophilic balance (HLB)  
111 of the particles can be adjusted, so the type of resulting  
112 emulsion (O-in-W or W-in-O) can be systematically changed.  
113 In contrast to regular emulsions stabilized by surfactant  
114 molecules, the stability of Pickering emulsions is greatly  
115 affected by different parameters. Among the most critical  
116 ones, we can mention composition of the organic and aqueous  
117 phases, contact angle among the water–solid–oil phases,  
118 particle size, particle concentration, and particle–particle  
119 interaction at the interface.<sup>17–255</sup>

120 According to theoretical calculations, confirmed by experimental  
121 results, stable emulsions are formed when the particle size is within  
122 the range of 0.01–1.0  $\mu\text{m}$ . Outside this range, stability is hindered  
123 by either flocculation (when particles are too large) or Brownian  
124 motion (when particles are too small).<sup>26–28</sup>

125 The effectiveness of particles in stabilizing emulsion droplets  
126 is strongly dependent on the extent of particle–particle inter-  
127 actions. For example, water-wetted particles tend to stabilize  
128 oil-in-water emulsions, while oil-wetted particles stabilize  
129 W-in-O emulsions. When they are mixed, their stabilizing action  
130 is neutralized, leading to a rapid coalescence of the emulsion  
131 droplets. Such observation suggests that the strength of the  
132 rigid film of particles at the water/oil interface depends signifi-  
133 cantly on the particle–particle interaction, which ultimately  
134 affects the emulsion stability.<sup>29</sup>

135 The composition of the oil and aqueous phases is also  
136 important in determining the type of emulsion, because the  
137 surface of the particles is sensitive to the adsorption of surface-  
138 active molecules that can change the HLB or wettability of the  
139 particle, as well as the concentration of ionic species in the  
140 aqueous phase that can modify the electrostatic interaction  
141 between particles and, in consequence, their state of  
142 aggregation.

Particle concentration is another important parameter that  
directly affects the volume fraction of emulsion, stability, and  
droplet size of Pickering emulsions.<sup>30–32</sup> Droplet size decreases  
with increasing particle concentration not only due to an  
increased interfacial area that accommodates more particles, but  
also due to the modification of rheological properties.<sup>33</sup> At low  
concentration of particles at the fluid/fluid interface, the  
viscosity coefficients dominate the rheological parameters.  
However, at high concentrations, elastic contributions become  
significant, due to particle–particle interaction. As a result, the  
fluid at the colloid-laden interface develops a viscoelastic or  
pseudo-plastic behavior.

In a recent study, we have demonstrated the stabilization of  
Pickering emulsions by nanohybrid particles composed of single-  
walled carbon nanotubes (SWCNT) and silica.<sup>34</sup> We showed that  
we could control the droplet size and the effective volume fraction  
of emulsion by simply adjusting the water/oil (W/O) ratio and  
the amount of nanohybrids. More recently, we further investigated  
the application of the concept to catalysis by incorporating active  
species on the surface of nanohybrids, which catalyze reactions at  
the oil/water interface.<sup>35</sup> Some of the reactions used to  
demonstrate the concept include metal-catalyzed hydrodeoxygen-  
ation and base-catalyzed aldol condensation of molecules with  
different solubilities, some water-soluble and some oil-soluble. The  
concept of “phase selectivity” was put forward by conducting  
hydrogenation on only one of the phases, while avoiding reaction  
in the other phase.<sup>36,37</sup>

In this contribution, we have investigated the application of  
nanohybrid particles that preferentially locate at the water/oil  
interface and catalyze different reactions (oxidation and hydro-  
genation), which may have an impact on EOR. In addition to the  
SWCNT/silica originally synthesized, different types of nano-  
hybrids were compared. Multiwalled carbon nanotubes  
(MWCNTs) grown on alumina, onion-like carbon (OC) on  
silica, and Janus amphiphilic particles were found to be very  
effective in acting as emulsion stabilizers and catalyst supports. The  
Janus particles are dissymmetrically functionalized silica nano-  
hybrids that present a structure containing a hydrophobic and a  
hydrophilic side.<sup>38</sup> We have recently investigated in detail the  
mobility of aqueous dispersions of these nanohybrids in porous  
media.<sup>39</sup> Mobility studies on glass beads and crushed Berea sand  
columns demonstrated that the synthesized nanohybrids success-  
fully flow through porous media, particularly with the aid of small  
amounts of polymer (e.g., 500 ppm polyacrylamide, PAM). When  
the column was presaturated with oil, about half of the particles  
passed through the column while the other half remained trapped  
by the oil/water interface due to their amphiphilic properties. The  
effect of pH, salt, polymer, and surfactant concentration was also  
studied and it was concluded that neither salinity nor pH have a  
significant effect on the stability or mobility of the dispersions. In  
contrast, the addition of surfactants improved the stability of the  
dispersions, but decreased the surface activity of the particles and  
the stability of the emulsions. Therefore, we can envision that this  
type of nanohybrids could propagate in the water flow through the  
porous media and reach the oil phase. At that point, they can  
preferentially adsorb at the oil/water interface, where, if properly  
loaded with an appropriate active species, they could catalyze a  
desired reaction.

## 2. EXPERIMENTAL SECTION

**2.1. Materials.** Nanohybrids of various characteristics were  
synthesized and used as supports for catalytically active species.  
Among the various nanohybrids investigated, SWCNTs were grown

on Co-Mo/SiO<sub>2</sub> catalysts using the CoMoCAT method developed by our group<sup>40–43</sup> and commercialized by Southwest Nanotechnologies Inc. (SWE<sup>NT</sup>). The as-produced SWCNT/silica are the original nanohybrids described in our previous work as novel emulsifiers and catalyst supports.<sup>34</sup> Variations of the same method resulted in nanohybrids with different characteristics. For example, MWCNT synthesized on an alumina support provided nanohybrids with a higher fraction of hydrophilic moieties. Moreover, a treatment with nitric acid was carried out on the MWCNT on alumina in order to increase the hydrophilic defects on the carbon nanotubes surface. Other carbon structures such as onion carbon were also deposited on silica supports. Finally, Janus-type amphiphilic particles were prepared by a method described by Perro et al.<sup>38</sup> All of these nanohybrids have been previously used as support for catalytic species in recent studies of our group.<sup>35–37</sup>

Different catalytic species (Pd, Cu, Cr, Co, and Fe) were impregnated on the various nanohybrids, using the corresponding nitrate salts (from Sigma–Aldrich) as promoters of the metal catalysts. All the catalysts were produced by incipient wetness impregnation of the different supports (i.e., the different types of nanohybrids) with aqueous solutions of the specific metal precursors (Cu, Pd, and other nitrates). The samples were dried overnight at a temperature of 80 °C and then calcined in air at 250 °C for 3 h.

Tetralin, decalin, and phenanthrene (from Sigma–Aldrich) were used as both the oil phase in the oil-in-water (O-in-W) emulsions and as the reactant in the various reactions investigated. The water used in the study was purified by means of two Cole Parmer ion exchangers in series. Emulsions were prepared by ultrasonication of the two liquid phases in the presence of the nanohybrids with a Fisher Scientific, 600 W, 20 kHz horn sonicator, operated at an amplitude of 25%, as previously described.<sup>34</sup>

**2.2. Reaction Studies.** Partial oxidation and hydrogenation reactions were carried out in a 50 cm<sup>3</sup> stirred reactor (Parr, Model 4590), operating in semibatch mode, with a constant flow of gas (air and hydrogen, respectively) while the liquid was kept under constant stirring in the reactor vessel. In each run, the selected amounts of oil, water, and nanohybrid catalysts were placed in the vessel. The emulsion then was formed as stated above and the reactor was assembled. After this, the system was pressurized with N<sub>2</sub> and heated while stirring at 225 rpm. For the partial oxidation reactions, once the desired pressure and temperature were reached, the reaction time was measured from the start of the reactant gas (air) flow. For the hydrogenation reactions, a water/decalin emulsion stabilized by the catalytic nanohybrid was first formed in the vessel. After purging the

lines with N<sub>2</sub>, the reduction of the catalyst was achieved by flowing 110 sccm of H<sub>2</sub> for 3 h at 200 psi and 100 °C. The pressure then was adjusted to 900 psi and 200 °C and the reaction time was measured from the injection of the substrate molecule (e.g., phenanthrene).

In both cases, after completing the desired reaction period, the system was cooled and depressurized, and the product liquid was filtered. Samples were taken from each phase for product quantification. Reaction products were analyzed in a gas chromatograph (Agilent 6890A series) with a flame ionization detection (FID) device, using a capillary column (HP-Innowax with a length of 60 m) and a gas chromatograph–mass spectrometer (Shimadzu, Model QP2010S). The interfacial tension between mixtures and pure compounds and water was measured on a drop shape analyzer (Minitec).

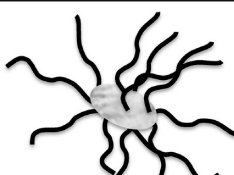



### 3. RESULTS AND DISCUSSION

**3.1. Interfacially Active Nanohybrids.** We have previously shown<sup>34–36</sup> that nanohybrid particles offer several advantages when used as emulsion stabilizers and catalyst supports:

- Higher activity is obtained for reactions occurring at the water/oil interface in biphasic systems due to the enhanced interfacial area;
- Reaction selectivity can be modified according to the solubility of the reactants in each phase;
- Product separation is facilitated due to differences in solubility; and
- Catalyst recovery can be readily accomplished by filtration.

In the present work, several nanohybrids have been used in the partial oxidation of tetralin: SWCNT/SiO<sub>2</sub>, MWCNT/Al<sub>2</sub>O<sub>3</sub>, onion carbon/SiO<sub>2</sub>, and Janus silica nanoparticles. For hydrogenation studies, Pd catalysts supported on nitric acid-functionalized MWCNT/Al<sub>2</sub>O<sub>3</sub> has been employed. Table 1 summarizes the characteristic features of the different nanohybrids, which have been tested for their ability to stabilize water/decalin emulsions. Figure 1 shows optical microscopy images of the emulsions produced with each one of the different nanohybrids at the same nanoparticle concentration of 3 mg/mL and a water/oil volume ratio of 1. As it can be

**Table 1. Schematic Description of the Different Nanohybrids Used as Emulsion Stabilizer and Support of Metal Clusters**

Type	Description	Schematic
Carbon / Oxide Nanoparticle Nanohybrids	(a) SWCNT/silica	
	(b) MWCNT/alumina	
	(c) Functionalized MWCNT/alumina	
	(d) Onion carbon/silica	
Janus Particles	(e) Partially-hydrophobized silica	



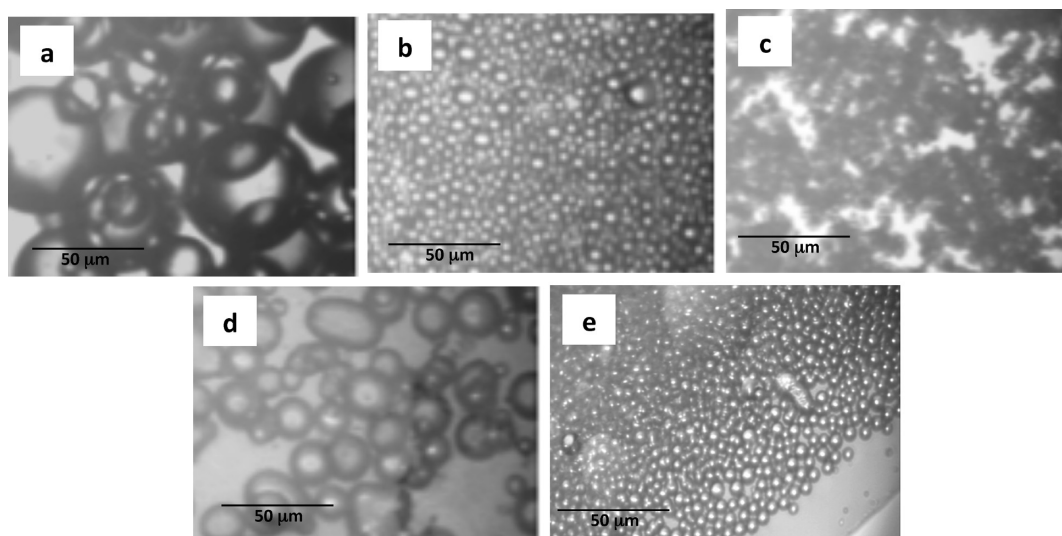


**Figure 1.** Optical microscopy images of the water/decalin emulsions stabilized by different nanohybrids (see Table 1): (a) SWCNT/SiO<sub>2</sub>, (b) MWCNT/Al<sub>2</sub>O<sub>3</sub>, (c) functionalized MWCNT/Al<sub>2</sub>O<sub>3</sub>, (d) onion carbon/SiO<sub>2</sub>, and (e) Janus silica nanoparticles.

observed, there are clear differences in the emulsions; under the conditions studied, the emulsions stabilized with SWCNT/SiO<sub>2</sub> and onion carbon/SiO<sub>2</sub> present bigger droplets (average size of 35 and 15 μm, respectively) than those stabilized with MWCNT/Al<sub>2</sub>O<sub>3</sub>, functionalized MWCNT/Al<sub>2</sub>O<sub>3</sub>, and Janus silica particles (8, 2, and 4 μm, respectively). The emulsion fraction also varies, being lower for SWCNT/SiO<sub>2</sub> and onion carbon/SiO<sub>2</sub> (10% and 30%, respectively) and reaching values of 50%, 85%, and 90% for MWCNT/Al<sub>2</sub>O<sub>3</sub>, functionalized MWCNT/Al<sub>2</sub>O<sub>3</sub>, and Janus silica particles, respectively. Thus, among all the nanohybrids investigated, functionalized MWCNT/Al<sub>2</sub>O<sub>3</sub> are the most effective nanohybrids for stabilizing emulsions, with high emulsion fractions and the smallest droplet sizes. The type of emulsion formed also is dependent on which nanohybrid is used, i.e., W-in-O for the SWCNT/SiO<sub>2</sub> and MWCNT/Al<sub>2</sub>O<sub>3</sub> emulsions, and O-in-W for the other three nanohybrids. This dependence of the type of emulsion with the nanohybrid used is directly related to the hydrophilic/lipophilic balance in the nanohybrids. It is well-known that more hydrophilic particles are preferentially wetted by water, which makes the interface bend concavely toward the oil, producing O-in-W emulsions, and vice versa.<sup>18,44,45</sup> Therefore, onion carbon/SiO<sub>2</sub> and Janus silica particles are more hydrophilic, while SWCNT/SiO<sub>2</sub> and MWCNT/Al<sub>2</sub>O<sub>3</sub> are more hydrophobic, because of their lower density of oxidized defects. The nitric acid treatment to the MWCNT/Al<sub>2</sub>O<sub>3</sub> creates hydrophilic defects on the surface of the carbon nanotubes, which makes the functionalized nanohybrids more hydrophilic and stabilizes O-in-W emulsions under the conditions studied.

In summary, comparing the behavior of the different nanohybrids (emulsion fraction and droplet size), it can be concluded that the resulting interfacial area follows the sequence: functionalized MWCNT/Al<sub>2</sub>O<sub>3</sub> > Janus silica particles > MWCNT/Al<sub>2</sub>O<sub>3</sub> > onion carbon/SiO<sub>2</sub> > SWCNT/SiO<sub>2</sub>.

Once the effectiveness of the nanohybrids for stabilizing emulsions was demonstrated, metal particles were deposited on their surface and used as catalysts for the partial oxidation of tetralin and the hydrogenation of polynuclear aromatics in emulsion systems. Figure 2 shows a schematic illustration of the

hydrogenation of polynuclear aromatics at the water/oil interface in the nanohybrid-stabilized emulsions. In the case of carbon nanotube based-nanohybrids, we have shown in a previous study that the carbon nanotubes are oriented toward the organic phase, while the metal oxide nanoparticles remain closer to the aqueous phase.<sup>35</sup>

The type of nanohybrids used also affects the dispersion of the metal particles. Figure 3 shows TEM images of the different nanohybrid-supported Pd catalysts in this work. Although the catalyst preparation conditions were identical in all cases (incipient wetness impregnation of the aqueous solution of the metal precursor), the size of the metal cluster varied with the type of nanohybrids used as support. That is, the average sizes of the Pd cluster were 4.9, 4.6, 3, 2.5, and 2.1 nm, for SWCNT/SiO<sub>2</sub>, onion carbon/SiO<sub>2</sub>, MWCNT/Al<sub>2</sub>O<sub>3</sub>, Janus silica particles, and functionalized MWCNT/Al<sub>2</sub>O<sub>3</sub>, respectively. The trend is clear: the higher the density of anchoring sites on the support, the higher the metal dispersion.

Having in mind a potential application in subsurface reservoirs, we studied the catalytic activity of several nanohybrids (see Table 2) for oxidation and hydrogenation reactions of interest in subsurface conversion. Figure 4 illustrates the concept of simultaneous injection of the aqueous dispersion of the nanoparticles and the gaseous reactant to react in situ for subsurface applications. As an example of a possible in situ reaction, the partial oxidation of hydrocarbons appears as a desirable conversion to increase the polarity of the oil molecules located at the interface. This conversion might significantly reduce the oil/water IFT, enhancing the capillary number. At the same time, if the oxidized molecules migrate to the water phase due to their enhanced water affinity, the viscosity of the mobilizing fluid will increase and, consequently, the sweeping efficiency of this fluid would improve.

**3.2.1. Partial Oxidation of Oil Constituents. Catalyst Activity.** Tetralin oxidation was carried out at 80 °C and 200 psi under a constant 200 sccm flow rate of air. The water/oil volume ratio in the liquid phase was 0.5, and the total volume was 30 mL. The total nanohybrid catalyst mass was 60 mg with a metal loading of 10 wt %. Different nanohybrid supports and different metals were used for this reaction. Table 2 summarizes

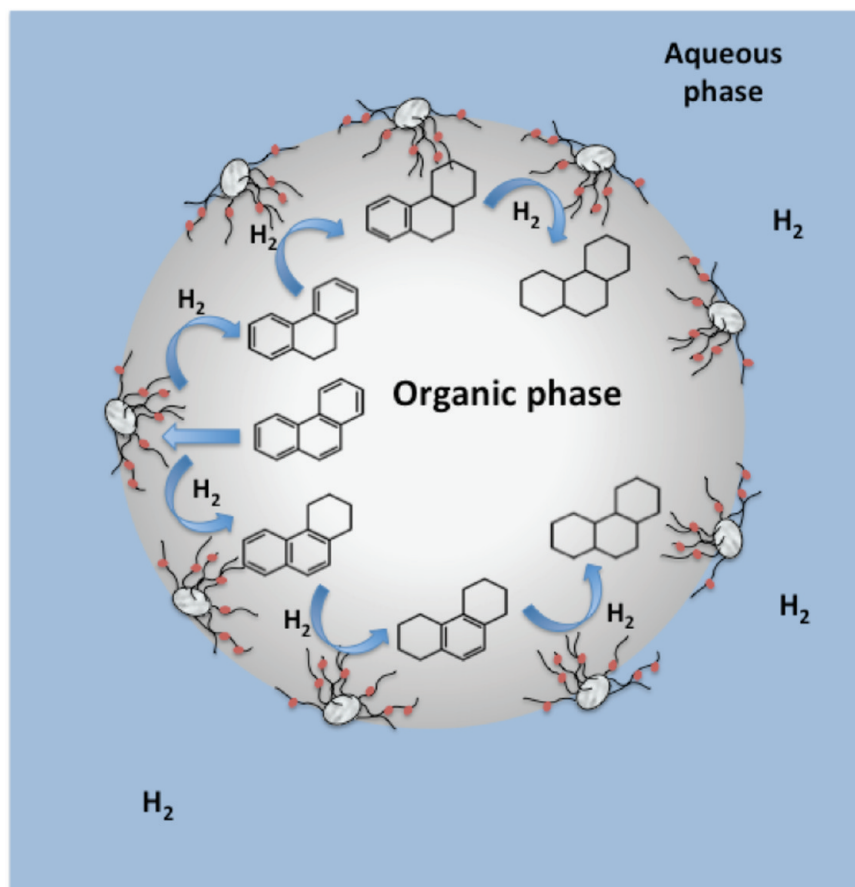


**Figure 2.** Schematic representation of the hydrogenation of phenanthrene at the water/oil interface in the nanohybrid-stabilized emulsions. The reactants and intermediate products are only soluble in the organic phase, while the hydrophobic part of the nanohybrids (CNT) contains most of the catalytically active species (Pd clusters).

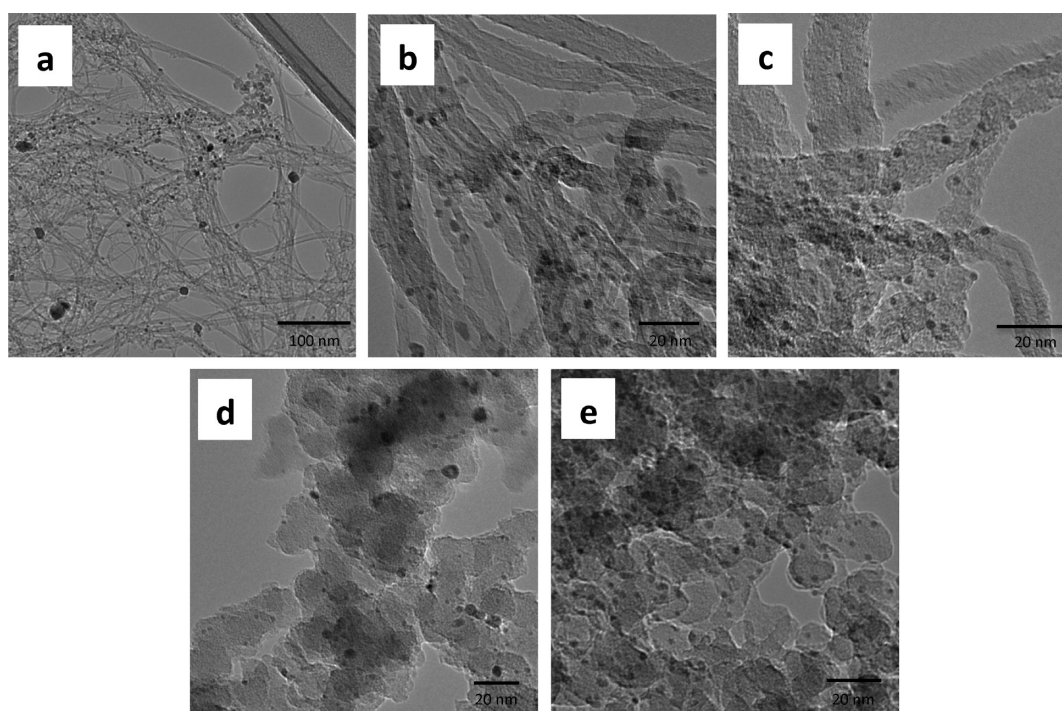


**Figure 3.** High-resolution TEM images of the catalysts prepared with 5 wt % Pd supported on different nanohybrids (see Table 1): (a) SWCNT/ $\text{SiO}_2$ , (b) MWCNT/ $\text{Al}_2\text{O}_3$ , (c) functionalized MWCNT/ $\text{Al}_2\text{O}_3$ , (d) onion carbon/ $\text{SiO}_2$ , and (e) Janus silica nanoparticles.

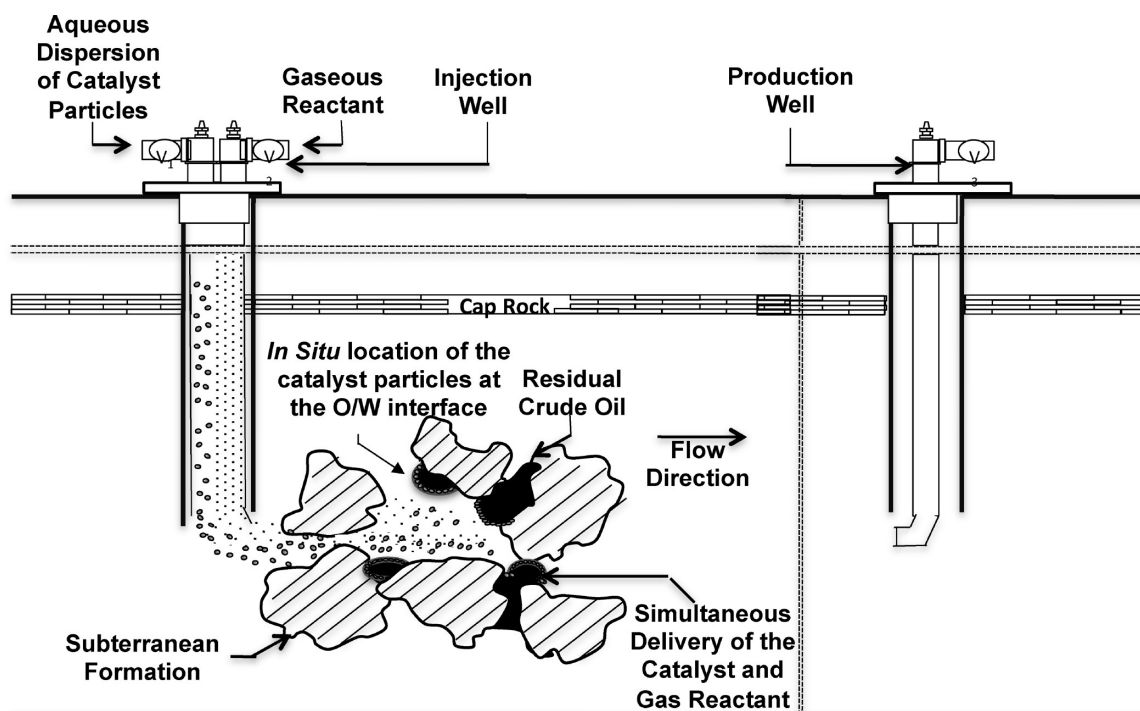


**Figure 4.** Representation of the introduction of the catalyst nanoparticles and the gaseous reactant in the wellbore for application in subsurface reservoirs.

**Table 2. Catalysts Tested on Tetralin Partial Oxidation**

metal	metal loading (wt %)
(a) Support: SWNT on Silica	
Pd	6, 10
Cu	6, 10
Fe	10
Cr	10
(b) Support: MWNT on Alumina	
Pd	10
Cu	10
(d) Support: Onion Carbon/Silica	
Pd	10
(e) Support: Janus Silica Nanoparticles	
Pd	10

**Table 3. Results for the Catalyst Screening for Tetralin Oxidation at 80 °C and 200 psi<sup>a</sup>**

metal	tetralin conversion (%)	Products Yield, Y (%)		Selectivity, S (%)	
		tetralone	tetralol	tetralone	tetralol
Pd	6.0	4.0	2.0	64	36
Cu	4.8	4.0	0.74	84	16
Fe	1.3	0.85	0.42	67	33
Cr	1.0	0.69	0.33	68	32
blank	0.49	0.35	0.14	71	29

<sup>a</sup>Conditions: reaction time, 24 h; O/W ratio, 0.5; total volume, 30 mL; catalyst weight, 60 mg; metal loading, 10 wt %; and air flow, 200 sccm. Support (a) (nanohybrid SWNT/silica) was used.

**Table 4. Comparison of Metal Loadings for the Cu, Pd on Catalysts on Support (a) (Nanohybrid SWNT/Silica) for Tetralin Oxidation at 80 °C and 200 psi<sup>a</sup>**

metal	metal loading (%)	tetralin conversion (%)	Selectivity, S (%)		Products Yield, Y (%)	
			tetralone	tetralol	tetralone	tetralol
Pd	6	3.0	68	32	2.0	0.96
	10	6.0	64	36	4.0	2.0
Cu	6	8.2	89	11	7.3	0.94
	10	4.8	84	16	4.0	0.74

<sup>a</sup>Conditions: reaction time, 24 h; O/W ratio, 0.5; total volume, 30 mL; catalyst weight, 60 mg; and air flow, 200 sccm. Support (a) (nanohybrid SWNT/silica) was used.

the characteristics of the catalysts tested in the partial oxidation reactions.

The activity of different metal catalysts loaded on the SWCNT/SiO<sub>2</sub> nanohybrids was tested under the same reaction conditions. A sample of bare nanohybrids without any metal was used as a blank for comparison. The tetralin conversion, product yields, and selectivities obtained over the various samples after a reaction period of 24 h are summarized in Table 3. The main products of the reaction are 1-tetralone and 1-tetralol, as previously reported,<sup>46–51</sup> with traces of naphthalene and dihydronaphthalene. The results clearly show that Pd and Cu lead to much higher conversions than the other metals. Regarding the selectivity toward the two possible products, Cu clearly displays the highest selectivity toward the ketone (84.5%). For this specific application, tetralone is the desired product, since it is more stable than the alcohol, which undergoes dehydration, losing its polarity.

With the two most active metals (Pd and Cu), different metal loadings (6 and 10 wt %) were compared. The results are presented in Table 4. For the Pd catalysts, an increase in

conversion with the metal loading is observed. In contrast, the Cu catalysts showed the opposite behavior, since it is probable that high metal loading in Cu catalysts leads to metal aggregation and, consequently, lower activity. Thus, runs at varying



reaction times were evaluated on the two most active materials, i.e., 10 wt % Pd and 6 wt % Cu supported on the SWCNT/SiO<sub>2</sub> nanohybrids.

Figure 5 shows that both metal catalysts exhibit similar activity evolution with reaction time. That is, the conversion is

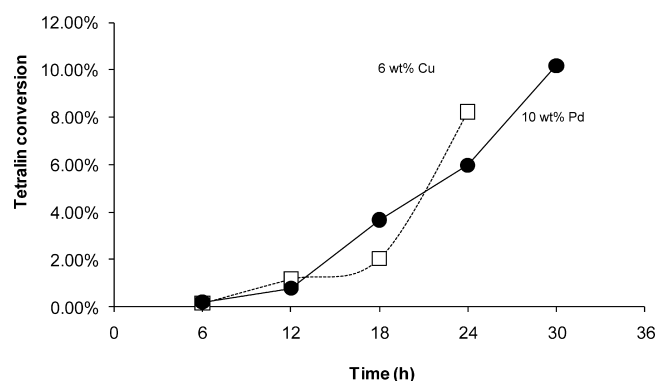


**Figure 5.** Conversion versus time for tetralin oxidation at 80 °C and 200 psi, using support (a) (nanohybrid SWNT/silica). Conditions: reaction time, 24 h; O/W ratio, 0.5; emulsion volume, 30 mL; catalyst weight, 60 mg; and air flow, 200 sccm.

initially negligible, with zero derivative at zero time, but the slope begins to increase with time, indicating an induction of activity. The induction period lasts for several hours, i.e., ~18 h for the Cu catalyst and ~24 h for the Pd catalyst. Similarly long induction periods have been previously observed in other partial oxidation reactions.<sup>51,52</sup> It is generally accepted that these induction periods are related to the rather slow generation of hydroperoxides. They are intermediates in this type of reactions, which typically involve a series of complex free radical steps. In the specific case of the oxidation of tetralin, it has been shown that a crucial intermediate is tetralin 1-hydroperoxide,<sup>52</sup> which readily decomposes to yield 1-tetralone and 1-tetralol, the two main products experimentally observed. As a result of this decomposition, the free radicals formed further attack tetralin, accelerating the overall reaction, which proceeds autocatalytically.<sup>52</sup>

Several nanohybrid supports were tested using Pd as the active metal with a loading of 10 wt %. The results on the different nanohybrids are compared in Table 5. It can be

**Table 5.** Result of the Reaction Using 10 wt % Pd Catalysts on Different Supports for Tetralin Oxidation at 80 °C and 200 psi<sup>a</sup>

nanohybrid support	tetralin conversion (%)	Selectivity, S (%)	
		tetralone	tetralol
(a) SWNT on silica	6.0	64	36
(b) MWNT on alumina	27.9	65	35
(d) onion carbon on silica	6.7	63	37
(e) silica Janus particles	30.2	59	41

<sup>a</sup>Conditions: reaction time, 24 h; O/W ratio, 0.5; total volume, 30 mL; catalyst weight, 60 mg; and air flow, 200 sccm. Support (a) (nanohybrid SWNT/silica) was used.

observed that the silica Janus particles and the MWCNT/alumina hybrids showed a 5-fold increase in activity, compared to the first generation of nanohybrids based on SWCNT on silica. This activity enhancement is mainly attributed to the

better capability of these particles of forming emulsions with smaller droplet sizes, resulting in a higher interfacial area than that obtained with the SWCNT on silica (see Figure 1). In addition, when comparing MWCNT to SWCNT and OC, the former has a better capability of anchoring Pd particles, because of the higher number of defects on their surface, which, as illustrated in Figure 3, provides active sites for metal deposition. The series of reactions over time using the MWCNT on alumina catalyst were carried out, and the results are shown in Figure 6. As stated before, the values of tetralin conversion and

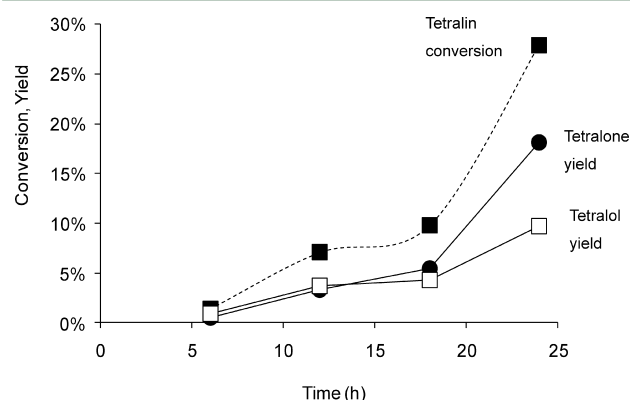


**Figure 6.** Conversion versus time for tetralin oxidation at 80 °C and 200 psi with 10 wt % Pd on MWNT/alumina catalyst. Conditions: O/W ratio, 0.5; emulsion volume, 30 mL; catalyst weight, 60 mg; and air flow, 200 sccm.

products yield are higher than those observed in Figure 5 for the SWCNT/silica catalysts. However, the activity induction period was still evident, since the conversion grew nonlinearly (e.g., 10% after the first 18 h of reaction, but 30% after 24 h).

Investigating ways to shorten the activation period, we found that, when the catalyst was prerduced in H<sub>2</sub>, the induction pattern changed drastically. For instance, a series of reactions was conducted at different reaction times, comparing the behavior of MWCNT/alumina-supported metal catalysts, with and without a pretreatment under a 200 sccm flow of H<sub>2</sub> at 80 °C and 200 psi for 3 h. The comparison is summarized in Figure 7 and clearly shows that prereducing the catalyst in H<sub>2</sub>

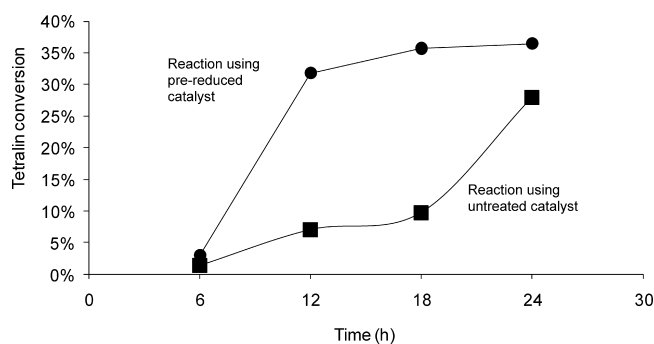


**Figure 7.** Comparison of activity of prerduced (3 h, 200 sccm H<sub>2</sub> flow at 80 °C and 200 psi) and untreated catalysts. Reaction conditions: 80 °C, 200 psi, and 10 wt % Pd metal loading on MWNT/alumina catalyst. O/W ratio = 0.5. Emulsion volume = 30 mL. Catalyst weight = 60 mg. Air flow = 200 sccm.

significantly shortens the induction period. It is evident that the prereducing activates the catalyst to a state that would take

much longer to be obtained under reaction conditions. For example, after 12 h of reaction, the conversion of tetralin on the pretreated catalyst is more than 4 times greater than on the untreated catalyst. However, after 24 h, the difference in conversion is much smaller. We believe that this difference in length of the induction period is due to the generation of the active sites by the prereduction step. It appears that the fully oxidized Pd species that result from the initial catalyst calcination under air are not active for partial oxidation, but rather partially reduced Pd species are needed for activity. The pretreatment seems to accelerate the formation of these species, which may provide sites for oxygen and/or tetralin adsorption. Under reaction without prereduction, these species may still form, but it seems to take much longer.

**3.2.2. Changes in Interfacial Tension After Reaction.** The interfacial tension of several mixtures of tetralin/tetralone and water was measured to verify that it decreases when oxidized polar groups (tetralone) are generated from the nonpolar phase (tetralin), which occurs under oxidation reaction. The measurements were compared to a model<sup>53</sup> that predicts an exponential decay with the concentration of polar species added to a nonpolar phase. As shown in Figure 8, the fitting is

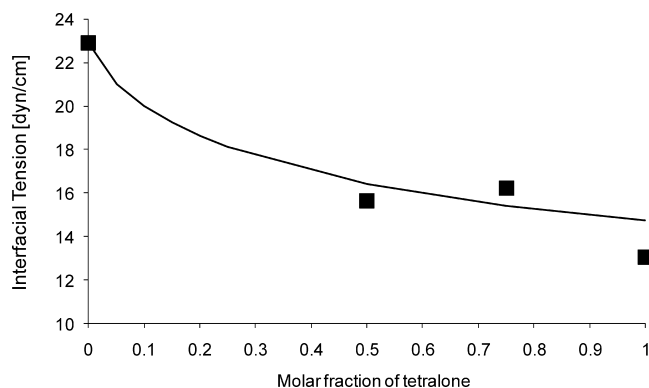


**Figure 8.** Interfacial tension between mixtures of tetralin/tetralone and water determined experimentally (symbols) and using the exponential model proposed by Kim and Burgess.<sup>53</sup> The mean absolute error is 0.8 dyne/cm (or 5.4%).

very good (obtaining a mean absolute error (MAE) of 0.83 dyne/cm and an average percentage error of 5.4%) and demonstrates that indeed, the addition of small amounts of tetralone generates a considerable decrease in interfacial tension. This decrease is caused by the enrichment of the polar compound at the oil/water interface, because of a higher affinity of the polar compound to water, compared to the nonpolar bulk phase.

Although the reduction in IFT shown in Figure 8 does not reach the typical reductions that one would expect for EOR techniques, it serves as an initial proof of concept for this application. If the oxidation reaction were carried out to convert molecules with lower polarity than that of tetralin, such as a long-chain olefin, the impact on the IFT reduction would be increased. Moreover, a potentially important advantage of the underground oxidation reactions in oil-wet reservoirs could be the modification of the wettability of the porous medium. If the catalytic nanoparticles migrate into the porous rock, they may catalyze the oxidation of the asphaltene-type deposits on the walls of the rock, thus changing their surface chemistry. One could anticipate that oxidized asphaltenes may convert the rock

wall from oil-wet to water-wet, which could have a huge impact in oil mobility.

Tetralin has been selected as a model compound representing the complex mixtures typically found in crude oil to simplify the experimental procedures required to analyze the results of the oxidation reactions. However, we have tested the activity of these catalysts in the presence of other aromatics, olefins, paraffins, and naphthenics, with no significant changes in the measured tetralin oxidation activity. Thus, it can be expected that the results reported here can be well-extrapolated to reactions with compositions similar to that of crude oil.

**3.3.1. Hydrogenation of Polynuclear Aromatics. Catalyst Activity.** For the study of hydrogenation reactions, MWCNT on alumina nanohybrids were pretreated with nitric acid (16 M) at 100 °C for 6 h to create anchoring sites at the MWCNT walls. With this particular pretreatment, the Pd nanoparticles become preferentially coordinated at the oxidized MWCNT sites,<sup>54</sup> since the density of defects on the MWCNT increases upon oxidation with nitric acid. This enhancement in the metal–support interaction improves the metal dispersion over the hydrophobic carbon nanotubes, which is responsible for the conversion of the hydrocarbons present in the organic phase. In addition, this oxidation treatment of the MWCNT/alumina also enhances the repulsive forces between MWCNT, because of the higher density of charge that is caused by the carboxylic acid groups. This repulsion results in a better dispersion of the nanoparticles in the liquid phase, increasing the emulsification efficiency of the nanohybrid.

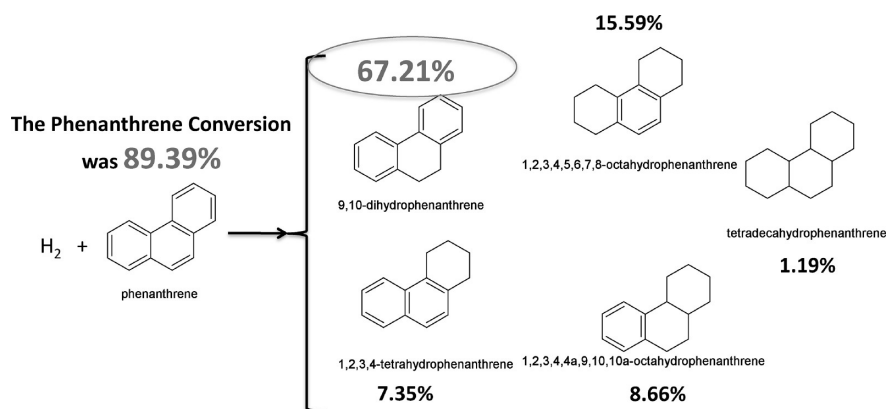
The hydrogenation reactions were run for 24 h at 200 °C and 900 psi under a constant 110 sccm flow of H<sub>2</sub>. The water/oil volume ratio in the mixture was kept equal to 1 and the total mass of catalytic nanohybrid of MWCNT(ox)/alumina was 30 mg. The active metal employed was Pd (5 wt %).

Figure 9 shows the different products obtained in the hydrogenation of phenanthrene over the 5 wt % Pd on MWCNT(ox)/alumina after a 24 h reaction period under 900 psi of H<sub>2</sub> and 200 °C, including the individual yields obtained at a total conversion of 89.39%. The main product was 9,10-dihydrophenanthrene (67.2% yield), followed by 1,2,3,4,5,6,7,8-octahydrophenanthrene (15.6% yield), 1,2,3,4,4a-octahydrophenanthrene (8.7% yield), and 1,2,3,4-tetrahydrophenanthrene (1.2% yield).

One of the possible effects of hydrogenation on rheological properties could be associated with the increased flexibility of the polyaromatic molecules when the aromaticity is broken. This interesting effect could explain the change of the state of matter observed when the phenanthrene (which is a solid at room temperature) is selectively hydrogenated toward the 9,10-dihydrophenanthrene (a liquid at room temperature). Hence, based on this observation, we decided to study the effect of the extent of hydrogenation of the polyaromatic molecules on the dynamic viscosity ( $\mu$ ).

For this analysis, we employed the known approach of combining experimental data with Quantitative Structure–Property Relationship (QSPR) software.<sup>55,56</sup> This method allowed us to predict the dynamic viscosity of molecules that are not commercially available. The QSPR software used for this purpose was MDL QSAR provided by MDL Information Systems, Inc. In this approach, experimental measurements of a given property, such as viscosity, become related to the molecular structure using linear models in terms of molecular descriptors (MD), which are readily calculated from the structure of the molecule.





**Figure 9.** Conversion and yields of the different products in the hydrogenation of phenanthrene over 5 wt % Pd on oxidized MWNT/alumina after 24 h of reaction under 900 psi of  $H_2$  and 200 °C.

The first step in this method is the construction of a database of the property of interest for molecules with similar structure to those of the unknown (e.g., aromatics, naphthenics, etc.). For building this database, we used viscosity data from the work of Ivanciuc et al.<sup>57</sup> for 27 polyaromatics and polynaphthenics. A model was generated with this set of molecules and tested by the cross-validation method, which confirmed that the training set was statistically reliable and, as demonstrated in Figure 10, it

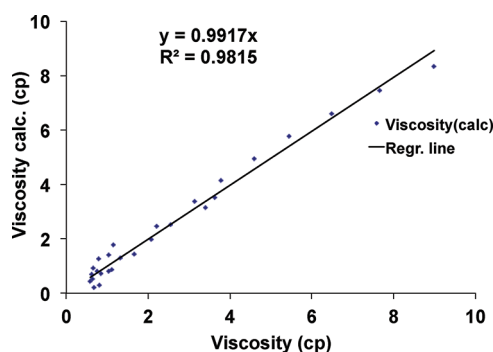


**Figure 10.** Validation of the QSPR model for the prediction of the viscosity of polyaromatic molecules ( $r^2 = 0.9817$ ; mean absolute error (MAE) = 0.26 cP).

was described very well by the regression equation shown below. The square correlation coefficient ( $r^2$ ), standard deviation (SD), and mean absolute error (MAE) of the resulting model (eq 1) were 0.9817, 0.3594 cP, and 0.26 cP, respectively.

$$\mu_{(cp)} = -20.23H_{\max \text{ pos}} - 11.05Q_v + 2.07x_2 - 8.61xp_9 + 6.48xvp_6 + 0.66SsCH_3 + 32.34 \quad (1)$$

where  $H_{\max \text{ pos}}$  is the largest E-state in a hydrogen atom in the molecule,  $Q_v$  the molecular and group polarity index,  $x_2$  the connectivity simple second-order chi index,  $xp_9$  the connectivity simple ninth-order path chi index,  $xvp_6$  the connectivity valence sixth-order path chi index, and  $SsCH_3$  the count of all the  $-CH_3$  groups in the molecules.

This model was used to predict the dynamic viscosity of the 9,10-dihydrophenanthrene, 1,2,3,4-tetrahydrophenanthrene, 1,2,3,4,4a-octahydrophenanthrene, 1,2,3,4,5,6,7,8-octahydrophenanthrene, and tetradecanohydrophenanthrene, and the results are shown in Table 6. Initially, the reduction of the side or central ring of the phenanthrene is enough to change the state of matter of the bulk phenanthrene from solid to liquid. This could be attributed to the change in the shape of the molecule, that, in the case of the phenanthrene, is completely flat, allowing the arrangement of the molecules in a crystal structure, while in the case of the 9,10-dihydrophenanthrene and 1,2,3,4-tetrahydrophenanthrene, the arrangement is less planar, with viscosities of 3.457 and 3.549 cP, respectively. Then, further hydrogenation of the phenanthrene yields to the 1,2,3,4,4a-octahydrophenanthrene (6.123 cP) and 1,2,3,4,5,6,7,8-octahydrophenanthrene (4.285 cP), with higher viscosities than those obtained during the first hydrogenation. This reverse effect in the dynamic viscosity could be ascribed to the increase of the dispersion forces between molecules and the larger molecular volume obtained upon hydrogenation. Finally, the complete hydrogenation of the phenanthrene to tetradecanohydrophenanthrene increases the viscosity up to 19.82 cP.

**3.3.3. Other Benefits of the Partial Hydrogenation.** In addition to the impact on the oil viscosity, partial hydrogenation is an effective pretreatment previous to the partial oxidation of the aromatic compounds. That is, partially hydrogenated aromatic compounds (e.g., tetralin) are more

**Table 6.** Change in the QSPR Molecular Descriptors and the Viscosity of Phenanthrene upon Hydrogenation Reaction of Phenanthrene

compound	Descriptors						property viscosity (cP)
	$H_{\max \text{ pos}}$	$Q_v$	$x_2$	$xp_9$	$xvp_6$	$SsCH_3$	
9,10-dihydrophenanthrene	1.2284	1.3272	5.9941	0.8958	0.9319	0.0000	3.54
1,2,3,4-tetrahydrophenanthrene	1.2114	1.437	5.9941	0.8958	1.0521	0.0000	3.45
1,2,3,4,5,6,7,8-octahydrophenanthrene	1.1424	1.7018	5.9941	0.8958	1.4162	0.0000	4.28
1,2,3,4,4a,9,10,10a-octahydrophenanthrene	1.1424	1.6528	5.9941	0.8958	1.6164	0.0000	6.12
tetrahydrophenanthrene	0.5191	2.1147	5.9941	0.8958	2.5777	0.0000	19.85

reactive toward partial oxidation than their saturated (e.g., decalin) and completely aromatic (e.g., naphthalene) counterparts. For example, while tetralin is readily oxidized under mild conditions (as shown in this work), decalin and naphthalene cannot even start to be oxidized. The main reason for this difference in activity is the presence of the  $\alpha$  carbon in the 1-position in tetralin. This C atom has two H atoms weakly bound, because of the resonance stabilization of the aromatic ring. Consistent with this, we observe that tetralin is only oxidized at the C1 position, and no products of partial oxidation at a different C atom are observed.

Furthermore, selective hydrogenation to target products could also be used to convert components in the oil phase of the emulsions to increase the viscosity of the sweeping fluid. As a result, this decrease in mobility ratio will result in enhancement of the oil recovery.

#### 4. CONCLUSIONS

From the results presented in this paper the following conclusions can be drawn:

- (1) In addition to be able to stabilize emulsions, the catalysts resulting from the deposition of metals on nanohybrid supports are active for both oxidation and hydrogenation of organic compounds at the oil/water interface.
- (2) The oxidation of aromatic compounds and hydrocarbons at the interface reduces the oil–water IFT, since the species with higher dipole moment (oxygenates) dominate the interface. The reduction of the IFT improves the capillary number, which should enhance the oil recovery.
- (3) The complete hydrogenation of the polyaromatic molecules increases the viscosity of the resulting products. The selective hydrogenation could be an appropriate strategy to increase the viscosity of the sweeping fluid (emulsion), improving the mobility ratio.
- (4) As a result, the combination of oxidation and hydrogenation reactions would enhance the oil recovery by simultaneously increasing the capillary number (decreasing the interfacial tension) and enhancing the mobility ratio (increasing the viscosity of the sweeping phase), with the same effect as the currently used injections of surfactant and polymer water solutions.

#### AUTHOR INFORMATION

##### Corresponding Author

\*Tel.: (405) 364-2773. E-mail: resasco@ou.edu.

##### Notes

The authors declare no competing financial interest.

#### ACKNOWLEDGMENTS

Funding was provided by the Department of Energy (DESC0004600) and the Advanced Energy Consortium (AEC; BP America, Baker Hughes, ConocoPhillips, Halliburton, Marathon, Occidental, Petrobras, Schlumberger, Shell, and Total).

#### REFERENCES

- (1) Standnes, D. C.; Austad, T. J. *J. Pet. Sci. Eng.* **2000**, *28*, 123–143.
- (2) Iglaier, S.; Wu, Y.; Shuler, P.; Tang, Y.; Goddard, W. A. III. *J. Pet. Sci. Eng.* **2010**, *71*, 23–29.

- (3) Ingram, D. R.; Kotsmar, C.; Yoon, K. Y.; Shao, S.; Huh, C.; Bryant, S. L.; Milner, T. E.; Johnston, K. P. *J. Colloid Interface Sci.* **2010**, *351*, 225–232.
- (4) Yu, H.; Kotsmar, C.; Yoon, K. Y.; Ingram, D. R.; Johnston, K. P.; Bryant, S. L.; Huh, C. Presented at the 17th SPE Improved Oil Recovery Symposium, Tulsa, OK, 2010; SPE Paper No. 129887.
- (5) Fletcher, A. J. P.; Davis, J. P. Presented at the 17th SPE Improved Oil Recovery Symposium, Tulsa, OK, 2010; SPE Paper No. 129531.
- (6) Ju, B.; Fan, T.; Ma, M. *China Particuol.* **1996**, *4*, 41–46.
- (7) Suleimanov, B. A.; Ismailov, F. S.; Veliyev, E. F. *J. Pet. Sci. Eng.* **2011**, *78*, 431–437.
- (8) Donaldson, E. C.; Chilingarian, G. V.; Yen, T. F. *Enhanced Oil Recovery, I: Fundamentals and Analyses*; Elsevier Science Publishing Company: New York, 1985; pp 47–63.
- (9) Abrams, A. *SPE J.* **1975**, *15*, 437–447.
- (10) Thomas, S.; Farouq Ali, S. M. *J. Pet. Sci. Eng.* **1989**, *3*, 121–136.
- (11) Simon, R. *Phys. Chem. Earth* **1981**, *13–14*, 447–460.
- (12) Satter, A.; Iqbal, G. M.; Buchwalter, J. L. *Practical Enhanced Reservoir Engineering: Assisted with Simulation Software*; PennWell Corporation: Tulsa, OK, 2007; pp 235–238.
- (13) Islam, M. R.; Farouq Ali, S. M. *J. Pet. Sci. Eng.* **1993**, *8*, 303–313.
- (14) Nasr-El-Din, H. A.; Taylor, K. C. In *Advances in Engineering Fluid Mechanics: Multiphase Reactor and Polymerization System Hydrodynamics*; Chermisinoff, N. P., Ed.; Gulf Publishing Company: Houston, TX, 1996; pp 615–668.
- (15) Kumar, R.; Dao, E.; Mohanty, K. K. Presented at the 17th SPE Improved Oil Recovery Symposium, Tulsa, OK 2010; SPE Paper No. 129914.
- (16) Skauge, T.; Spildo, K.; Skauge, A. Presented at the 17th SPE Improved Oil Recovery Symposium, Tulsa, OK 2010; SPE Paper No. 129933.
- (17) Binks, B. P.; Lumsdon, S. O. *Langmuir* **2001**, *17*, 4540–4547.
- (18) Binks, B. P.; Lumsdon, S. O. *Phys. Chem. Chem. Phys.* **1999**, *1*, 3007–3016.
- (19) Binks, B. P.; Lumsdon, S. O. *Langmuir* **2000**, *16*, 2539–2547.
- (20) Binks, B. P.; Lumsdon, S. O. *Phys. Chem. Chem. Phys.* **2000**, *2*, 2959–2967.
- (21) Ashby, N. P.; Binks, B. P. *Phys. Chem. Chem. Phys.* **2000**, *2*, 5640–5646.
- (22) Binks, B. P.; Clint, J. H. *Langmuir* **2002**, *18*, 1270–1273.
- (23) Giermanska-Kahn, J.; Schmitt, V.; Binks, B. P.; Leal-Calderon, F. *Langmuir* **2002**, *18*, 2515–2518.
- (24) Binks, B. P.; Kirkland, M. *Phys. Chem. Chem. Phys.* **2002**, *4*, 3727–3733.
- (25) Paunov, V. N.; Binks, B. P.; Ashby, N. P. *Langmuir* **2002**, *18*, 6946–6955.
- (26) Bowman, C. W. In *Proceedings of the 7th World Petroleum Congress*, Mexico City, Mexico, April 2–8, 1967; Vol. 3, pp 583–604.
- (27) Schulman, J. H.; Leja, J. *Trans. Faraday Soc.* **1954**, *50*, 598–605.
- (28) Binks, B. P.; Lumsdon, S. O. *Langmuir* **2001**, *17*, 4540–4547.
- (29) Lucassen-Reynders, E. H.; Van den Tempel, M. *J. Phys. Chem.* **1962**, *67*, 731–734.
- (30) Tambe, D. E.; Sharma, M. M. *J. Colloid Interface Sci.* **1993**, *157*, 244–253.
- (31) Aveyard, R.; Binks, B. P.; Clint, J. H. *Adv. Colloid Interface Sci.* **2003**, *100*, 503–546.
- (32) Arditty, S.; Whitby, C. P.; Binks, B. P.; Schmitt, V.; Leal-Calderon, F. *Eur. Phys. J.* **2003**, *11*, 273–281.
- (33) Tambe, D. E.; Sharma, M. M. *J. Colloid Interface Sci.* **1994**, *52*, 1–63.
- (34) Shen, M.; Resasco, D. E. *Langmuir* **2009**, *25*, 10843–10851.
- (35) Crossley, S.; Faria, J.; Shen, M.; Resasco, D. E. *Science* **2010**, *327*, 68–72.
- (36) Faria, J.; Ruiz, M. P.; Resasco, D. E. *Adv. Synth. Catal.* **2010**, *352*, 2359–2364.
- (37) Ruiz, M. P.; Faria, J.; Shen, M.; Drexler, S.; Prasomsri, T.; Resasco, D. E. *ChemSusChem* **2011**, *4*, 964–974.
- (38) Perro, A.; Meunier, F.; Schmitt, V.; Ravaine, S. *Colloids Surf., A* **2009**, *332*, 57–62.

- (39) Villamizar, L.; Lohateeraparp, P.; Harwell, J.; Resasco, D. E.; Shiau, B. Presented at the *17th SPE Improved Oil Recovery Symposium*, Tulsa, OK, 2010; SPE Paper No. 129901.
- (40) Kitiyanan, B.; Alvarez, W. E.; Harwell, J. H.; Resasco, D. E. *Chem. Phys. Lett.* **2000**, *317*, 497–503.
- (41) Alvarez, W. E.; Kitiyanan, B.; Borgna, A.; Resasco, D. E. *Carbon* **2001**, *39*, 547–558.
- (42) Resasco, D. E.; Alvarez, W. E.; Pompeo, F.; Balzano, L.; Herrera, J. E.; Kitiyanan, B.; Borgna, A. *J. Nanopart. Res.* **2002**, *4*, 131–136.
- (43) Alvarez, W. E.; Pompeo, F.; Herrera, J. E.; Balzano, L.; Resasco, D. E. *Chem. Mater.* **2002**, *14*, 1853–1858.
- (44) Binks, B. P. *Curr. Opin. Colloid Interface Sci.* **2002**, *7*, 21–41.
- (45) Binks, B. P.; Fletcher, P. D. I. *Langmuir* **2001**, *17*, 4708–4710.
- (46) Saratov, I. Y.; Simanov, V. A.; Golovanenko, B. I.; Saratova, S. D. *Pet. Chem.* **1968**, *8*, 59–67.
- (47) Martan, M.; Manassen, J.; Vofsi, D. *Tetrahedron* **1970**, *26*, 3815–3827.
- (48) Kamneva, A. I.; Zakharova, V. I.; Piteriskii, L. N.; Seleznev, V. A.; Artemov, A. V. *Pet. Chem.* **1975**, *15*, 98–106.
- (49) Mizukami, F.; Horiguchi, Y.; Tajima, M.; Imamura, J. *Bull. Chem. Soc. Jpn.* **1979**, *52*, 2689–2695.
- (50) Chung, Y. M.; Kang, K. K.; Ahn, W. S.; Lim, P. K. *J. Mol. Catal. A: Chem.* **1999**, *137*, 23–29.
- (51) Llabrés i Xamena, F. X.; Casanova, O.; Galiasso Tailleur, R.; Garcia, H.; Corma, A. *J. Catal.* **2008**, *255*, 220–227.
- (52) Robertson, A.; Waters, W. A. *Trans. Faraday Soc.* **1946**, *42*, 201–210.
- (53) Kim, H.; Burgess, D. J. *Colloid Interface Sci.* **2001**, *241*, 509–513.
- (54) Prasomsri, T.; Shi, D.; Resasco, D. E. *Chem. Phys. Lett.* **2010**, *497*, 103–107.
- (55) Crossley, S. P.; Alvarez, W. E.; Resasco, D. E. *Energy Fuels* **2008**, *22*, 2455–2464.
- (56) Resasco, D. E.; Crossley, S. *AIChE J.* **2009**, *55*, 1082–1089.
- (57) Ivanciuc, O.; Ivanciuc, T.; Filip, P. A.; Cabrol-Bass, D. *J. Chem. Inf. Comput. Sci.* **1999**, *39*, 515–524.